Modeling Heart Rate Regulation—Part I: Sit-to-stand Versus Head-up Tilt

Mette S. Olufsen, **April V. Alston**, and **Hien T. Tran**
Department of Mathematics, North Carolina State University, Campus Box 8205, Raleigh, NC 27695, USA e-mail: msolufse@math.ncsu.edu

Johnny T. Ottesen
Department of Mathematics and Physics, Roskilde University, Roskilde, Denmark

Vera Novak
Department of Gerontology, Beth Israel Deaconess Medical Center, Harvard Medical School, Boston, MA, USA

Abstract

In this study we describe a model predicting heart rate regulation during postural change from sitting to standing and during head-up tilt in five healthy elderly adults. The model uses blood pressure as an input to predict baroreflex firing-rate, which in turn is used to predict efferent parasympathetic and sympathetic outflows. The model also includes the combined effects of vestibular and central command stimulation of muscle sympathetic nerve activity, which is increased at the onset of postural change. Concentrations of acetylcholine and noradrenaline, predicted as functions of sympathetic and parasympathetic outflow, are then used to estimate the heart rate response. Dynamics of the heart rate and the baroreflex firing rate are modeled using a system of coupled ordinary delay differential equations with 17 parameters. We have derived sensitivity equations and ranked sensitivities of all parameters with respect to all state variables in our model. Using this model we show that during head-up tilt, the baseline firing-rate is larger than during sit-to-stand and that the combined effect of vestibular and central command stimulation of muscle sympathetic nerve activity is less pronounced during head-up tilt than during sit-to-stand.

Keywords

Mathematical modeling; Heart rate regulation; Sensitivity analysis

Introduction

Short-term cardiovascular regulation is often studied by imposing orthostatic stress challenges such as head-up tilt or sit-to-stand tests. During both passive (head-up tilt) and active standing (sit-to-stand) blood is pooled in the lower extremities due to gravitational forces. As a result, venous return is reduced, which leads to a decrease in cardiac stroke volume, a decline in arterial blood pressure, and an immediate decrease of blood flow to the brain. The reduction in arterial blood pressure unloads the baroreceptors located in the carotid and aortic walls, which leads to parasympathetic withdrawal and sympathetic activation through baroreflex-mediated autonomic regulation. Parasympathetic withdrawal induces a fast (within 1–2 cardiac cycles) increase in heart rate, while sympathetic activation yields a slow (within 6–8 cardiac cycles) increase in vascular resistance, vascular tone, cardiac contractility, and a further increase in heart rate (Smith and Kampine 1990; Guyton and Hall 1996). The main differences between head-up tilt and sit-to-stand are: (i) Head-up tilt was carried out using a slow-tilt procedure: it takes 5–10 s to tilt the subject from supine to standing, thus regulatory response

is activated before the subject is fully tilted. In addition since the procedure is passive, it requires limited muscle activity. Finally, due to the tilt-angle, gravitational forces act between the head and the torso leading to a transient decrease of intracranial pressure and increased venous draining from cerebral circulation to the heart. Simultaneously forces act between the torso and the lower body, leading to increased venous pooling in to the lower body. With these two mechanisms, venous return to the heart from cerebral circulation may transiently increase, while venous return from the periphery to the heart is decreased. These processes in turn affect beat-to-beat blood pressure and baroreflex firing-rate. (ii) The sit-to-stand occurs rapidly over 1–5 s and requires active muscle contraction and engagement of "central command" for movement initiation, which leads to an immediate increase in heart rate as the subject contracts his/her muscles to initiate standing (Olufsen et al. 2006). This increase in heart rate is observed before the initial drop in blood pressure and is possibly activated by combined effects of vestibular and central command stimulation of muscle sympathetic nerve activity.

Previous studies have demonstrated a strong vestibular stimulation of muscle sympathetic nerve activity in response to postural change, primarily in response to headdown rotation (Ray 2000;Ray and Monahan 2002;Ray and Carter 2003). However, a recent study in conscious cats show vestibular stimulation during head-up tilt (Wilson et al. 2006), and previous work by Kaufmann et al. (2002) suggests that the vestibular sympathetic reflex, originating in the otolith organs, may be one of the earliest mechanisms to be activated to sustain blood pressure upon standing. Studies analyzing vestibular stimulation of muscle sympathetic nerve activity using head-down rotation indicate that the vestibular system is activated independently of the baroreflex response, and that the two responses may be additive (Ray 2000;Ray and Carter 2003). Typically these responses have been studied by analyzing systemic measurements of blood pressure obtained using a Finapres device positioned at the level of the heart and heart rate obtained from analysis of ECG signals (Low 1997;Robertson et al. 2005). The majority of these experimental studies analyzed data using linear response models. For example, baroreflex sensitivity (Robbe et al. 1987;Johnson et al. 2006) has been assessed using spectral transfer functions relating changes in systolic blood pressure to interbeat intervals. This method is limited to analysis of relationships between two signals. Another limitation is that these data analysis methods lack the ability to predict how changes in neural responses interact to maintain arterial blood pressure.

In a previous study (Olufsen et al. 2006), we showed that a model for sit-to-stand clearly distinguishes between the baroreflex and vestibular/central command stimulation, we also showed significant differences between three groups of healthy young, healthy elderly and hypertensive elderly subjects. In addition, we were able to identify all 17 model-parameters using an inverse least-squares formulation. To solve the least squares problem we used the Nelder-Mead method, which is based on the simplex algorithm. However, we did not analyze the model in further detail or compared it to the response observed during head-up tilt. Furthermore, we lacked measures indicating how good our parameter estimates were. Also, we did not investigate which parameters were sensitive and which were not. In this study we derive sensitivity equations, which enable us to better understand the importance of each element in the model. We also compare computations from sit-to-stand where the vestibular system is believed to be an important contributor to the heart rate regulation with computations from head-up tilt, where the vestibular system appears to be engaged to a lesser degree. Another important issue is the methodologies for parameter estimation. The model proposed in (Olufsen et al. 2006) and studied further here has 17 parameters, and we have limited information about these parameters. Therefore, in a second part of this study we will analyze a number of optimization techniques used to identify model parameters.

Methods

Experimental Design

We analyzed data from five healthy elderly subjects (two woman and three men) aged 55–75 years (mean 60 ± 7 years), which participated in both sit-to-stand and headup tilt protocols. The subjects had no medical history of and were not treated for any systemic diseases, they did not take any cardiovascular active medications, had no history of head or brain injury, and had no history of more than one episode of syncope. Each subject was instrumented with a three-lead ECG to obtain heart rate. A photoplethysmographic device on the middle finger of the non-dominant hand was used to obtain noninvasive beat-to-beat blood pressure (Finapres device, Ohmeda Monitoring Systems, Englewood, Colorado). To eliminate effects of gravity, the hand was held at the level of the right atrium and supported by a sling. All physiological signals were digitized at 500 Hz using Labview NIDAQ software (National Instruments, Austin, TX) and stored for offline analysis. Times indicating the start of every cardiac cycle were extracted from the ECGs sampled at 500 Hz and validated off line. Blood pressure data were down-sampled to 50 Hz before being used as input to the mathematical model. Sit-to-stand protocol: After instrumentation, subjects sat in a straightbacked chair with their legs elevated at 90° in front of them. After 5 min of stable recordings, the subjects were asked to stand-up. Standing was defined as the moment both feet touched the floor, recorded by a force platform. Head-up tilt protocol: The subjects rested in supine position on the table for 10 min. Then, the table was tilted to 70° for 10 min. All subjects provided informed consent approved by the Institutional Review Board at Beth Israel Deaconess Medical Center, Boston, MA.

Modeling

In the analysis here we used the model put forward in (Olufsen et al. 2006). This model predicted heart rate using a chain of responses as illustrated in Fig. 1. Note that the model is sequential, i.e., all elements are linked in a chain. This allows for simpler implementation of the system of delay differential equations. Input to the model is the weighted mean blood pressure, which can be computed as

$$\overline{p}(t) = \alpha \int_{-\infty}^{t} p(s) e^{-\alpha(t-s)} ds \Rightarrow \frac{dp}{dt} = \alpha(p - \overline{p}).$$

1

The parameter α is the weight. A large value of α gives rise to a small weight of the past time (short memory), while a small value of α gives a larger weight (long memory). The weighted mean pressure $\overline{p}$ is a function of time, which oscillates with the same frequency as the instantaneous pressure p, but with a smaller amplitude, see Fig. 2.

As shown in Fig. 1, the mean blood pressure is used as an input to predict baroreflex firing-rate. Similar to previous work (Ottesen 1997; Olufsen et al. 2006) firing-rate is determined using a nonlinear differential equations of the form

$$\frac{dn_i}{dt} = k_i \frac{dp}{dt} \frac{n(M-n)}{(M/2)^2} - \frac{n_i}{\tau_i}, \quad i = S, I, L$$
$$n = n_S + n_I + n_L + N,$$

2

where n_i [1/s] denotes the firing-rate with $i = S, I, L$ accounting for short, intermediate, and long thresholds for the different receptors, $\overline{p}$ [mmHg] denotes the weighted mean blood pressure. This equation has a total of eight parameters: k_i [1/mmHg] are gain constants, $M = 120$ [1/s] is the maximal firing-rate, N [1/s] denotes the baseline firing-rate, and τ_i [s] are

characteristic times related to resetting. The baseline firing-rate N cannot exceed the maximum firing-rate and we assume that $N > M/2$. To enforce these bounds we have parameterized N using a sigmoid function of the form

$$N = \frac{M}{2} + \frac{\eta^2}{1+\eta^2}\left(M - \frac{M}{2}\right),$$

3

where η is an unknown parameter. The baroreceptor firingrate model in (2) exhibits nonlinear characteristics: it increases with increased carotid pressure and the response exhibits, hysteresis, threshold, and saturation. We use the term hysteresis to describe the nonlinear phenomenon between two quantities, the change in pressure ($d\overline{p}/dt$) and the change in firing-rate (dn_i/dt) described by Eq. 2. If $d\overline{p}/dt > 0$, then the two terms in the equation work in opposite direction yielding a smaller net derivative of dn_i/dt. However if $d\overline{p}/dt < 0$, then the two terms work in the same direction yielding a larger net derivative of dn_i/dt. This dynamic response agree with experimental studies, which suggest that a sufficiently fast decrease in pressure causes a step change in firing-rate followed by a resetting (adaptation) phenomenon and that the response to a decrease in pressure is faster than the response to an increase in pressure (Poitras et al. 1966;Spickler and Kedzi 1967;Franz 1969;Srinivasen and Nudelman 1972;Cecchini et al. 1982;Taher et al. 1988).

Using the baroreflex firing-rate n we predict the sympathetic and the parasympathetic outflows. The parasympathetic outflow T_{par} is proportional to the firingrate whereas sympathetic outflow T_{sym} is inversely related to the firing-rate (Danielsen and Ottensen 1997; Ottesen 1997). The sympathetic response is delayed 6–8 cardiac cycles; furthermore, an increased parasympathetic response dampens the sympathetic response (Levy and Zieske 1969). Finally, we accounted for additional activation $u(t)$ mediated by muscle sympathetic nerves and by central command. Combining all effects discussed above gives the following models for parasympathetic and sympathetic outflows

$$T_{par} = \frac{n(t)}{M},$$
$$T_s = 1 - \frac{n(t - \tau d)}{M} + u(t) \text{ giving } T_{sym} = \frac{T_s}{1 + \beta T_{par}}.$$

4

Parameters in these expressions include τ_d [s], the delay of the sympathetic response, and β, which is the parasympathetic dampening factor. The activation function $u(t)$ is represented by a quadratic impulse function of the form

$$u(t) = -[b(t - t_m)]^2 + u_0, \quad b = \sqrt{\frac{4u_0}{t_{per}^2}} \text{ and }$$
$$t_m = t_{start} + \frac{t_{per}}{2}.$$

5

This equation has three parameters, u_0 the amplitude of the response, t_{start}, and t_{per} the start time and duration of the response. A detailed description of the impulse function can be found in (Olufsen et al. 2006).

Using the sympathetic and parasympathetic outflows, nondimensionalized concentrations of acetylcholine C_{ach} and noradrenaline C_{nor} were computed from the first order equation

$$\frac{\mathrm{d}C_i}{\mathrm{d}t} = \frac{-C_i + T_j}{\tau_i}, \ i = sym, par, \ j = nor, ach,$$

6

where the parameters τ_{nor}, τ_{ach} [s] denote characteristic time scales for noradrenaline and acetylcholine. It should be noted that when $i = sym$ then $j = nor$ and when $i = par$ then $j = ach$. In this equation we have lumped the long chain of bio-chemical reactions into one first order reaction equation and taken the accumulated release time to be equal to the average clearance and consumption time for the respective substances. The heart rate potential was computed using an integrate and fire model of the form

$$\frac{\mathrm{d}\phi}{\mathrm{d}t} = H_0 \left(1 + M_s C_{nor} - M_P C_{ach}\right).$$

7

When $\phi = 1$ the heart beats and the interbeat interval (R–R interval, see Fig. 3) is taken as the time from $\phi = 0$ to $\phi = 1$. Then heart rate is found as the inverse of the interbeat interval. The parameter H_0 denotes intrinsic heart rate. Several studies have shown that intrinsic heart rate vary with age. Following ideas proposed in studies by Jose and Opthof et al. (Jose and Collison 1970; Opthof 2000) we let $H_0 = 1.97 - 9.50 \cdot 10^{-3} \times age$ [bps]. These studies assessed intrinsic heart rate under simultaneous presence of propranolol and atropine in 432 subjects and used linear regression to relate heart rate and age. This relation was also confirmed in a nonpharmacological study in cardiac transplant recipients (Strobel et al. 1999). The remaining parameters M_S and M_P represent the strength of the response to changes in the concentrations. To bound heart rate within physiological values, we constrained M_S and M_P in the interval [0,1]. This was done by introducing the parameters ξ_S and ξ_P so that

$$M_s = \frac{\xi_s^2}{1 + \xi_s^2} \ \text{and} \ M_P = \frac{\xi_P^2}{1 + \xi_P^2}.$$

8

In summary, the heart rate model proposed for this study can be written as a system of nonlinear delay differential equations of the form

$$\frac{\mathrm{d}x}{\mathrm{d}t} = f\left(\overline{x}(t), \overline{x}(t - \tau_d), \theta\right), \ \text{where}$$
$$\overline{x} = [p, n_s, n_I, n_L, C_{nor}, C_{ach}, \phi] \ \text{and}$$
$$\theta = \left[\alpha, k_s, k_I, k_L, \tau_S, \tau_I, \tau_L, \eta, \beta, u_0, t_{start}, t_{per}, \tau_d, \tau_{nor}, \tau_{ach}, \xi_s, \xi_P\right].$$

9

In the above system of equations $\overline{x}$ contains the seven state variables and θ contains the 17 model-parameters to be identified. Note that the model contains one more parameter (the maximum firing-rate $M = 120$ [1/s]), however, in this study we do not attempt to identify M. Initial values for the state variables and model parameters were estimated from physiological conditions. Table 4 lists all states and parameteres.

To validate this model against data we used Kelley's implementation of the Nelder–Mead optimization method (Kelley 1999) that minimizes the least-squared error J between computed $HR^c(t_i)$ and measured $HR^d(t_i)$ values of heart rate. We defined the least squares cost J by

$$J = \frac{1}{N_d} \sum_{i=1}^{N_d} (HR^c(t_i) - HR^d(t_i))^2.$$

10

In this equation N_d denotes the number of measurements of heart rate.

Initial iterates for all parameter values were determined using results from previous work (Olufsen et al. 2006). Thus, the initial iterate for the weighting parameter was set to $\alpha = 1$ [1/s], the firing-rate scaling parameters were set to $k_S = k_L = 2$, and $k_I = 1.5$ [1/mmHg s], and the timescales were set to $\tau_S = 1$, $\tau_I = 5$, and $\tau_L = 250$ [s]. Initial iterates for the parasympathetic and sympathetic time scales and the sympathetic delay were given by $\tau_{nor} = \tau_{ach} = 1$, $\tau_d = 7$ [s] and the parasympathetic damping of sympathetic outflow was set to $\beta = 1$. The initial iterates for the impulse function were amplitude, $u_0 = 1$, and the duration, $t_{per} = 5$ [s]. The start times t_{start} [s] were obtained from the experimental data. This parameter value indicates the time of initiation of standing and tilting, respectively.

Initial iterates for the parameters ξ_S and ξ_P used to determine M_S and M_P were calculated such that complete parasympathetic withdrawal ($C_{ach} = 0$) and maximal sympathetic stimulation ($C_{nor} = 1$) resulted in maximal heart rate $H_{max} = 3.62 - 1.42 \cdot 10^{-2} \times$ age [bps], while complete sympathetic inhibition ($C_{nor} = 0$) and maximal parasympathetic stimulation ($C_{ach} = 1$) resulted in "minimal" heart rate $H_{min} = 0.75$ [bps]. These considerations gave

$$\xi_s = \sqrt{\frac{H_{max} - H_0}{2H_0 - H_{max}}}, \; \xi_P = \sqrt{\frac{H_0 - H_{min}}{H_{min}}}.$$

11

It should be noted that in previous work (Olufsen et al. 2006) we did not account for the age-dependence when calculating maximal and intrinsic heart rates. The final initial iterate is for the parameter η, which is used to estimate the baseline firing-rate N. To estimate this value, we let the potential $d\phi/dt = H_r$, where H_r is the resting heart rate found by averaging the first five cardiac cycles. Then we solved for N, and used (4) to determine η as

$$\eta = \sqrt{\frac{2N-M}{2M-2N}}, \text{ where}$$
$$N = M\left(-b + \sqrt{b^2 - 4ac}\right)/(2a),$$
$$a = -M_P, b = 1 - \frac{H_r}{H_0} - M_S - M_P, c = M_S + 1 - \frac{H_r}{H_0}.$$

12

It should be emphasized that the considerations discussed above give rise to a set of initial iterates for the model parameters, which are within physiological range for each subject studied. To obtain individual patient specific parameter values that accurately predict dynamics observed for a given subject we performed non-linear optimization, identifying a set of parameters that minimize the least squares error between the computed and measured values of heart rate.

Numerical Considerations

The equations discussed above were solved using Matlab's built in differential equations solver *ode15s*. This solver is designed to solve stiff-differential equations using a variable order multistep method based on numerical differentiation formulas (Shampine and Reichelt 1997; Shampine et al. 1999).

The system of Eqs. 1–8 includes a delay variable (τ_d) used when calculating sympathetic outflow T_{sym} ($n(t - \tau_d)$). Thus, the differential equations cannot explicitly be solved using *ode15s*. Matlab does have a delay differential equations solver *dde23* based on a 2–3'rd order Runge–Kutta method. However, this method cannot handle stiff equations, thus we could not use it for the model discussed here. Now, it is possible to avoid implementing a stiffdelay solver, by taking advantage of the sequential structure of the model (see Fig. 1). To do so we first solve and store numerical values for $\overline{p}$ and n and then use the stored values for both $n(t)$ and $n(t - \tau_d)$ to compute parasympathetic and sympathetic outputs as described in Eqs. 4–8. Initial conditions used for this study are similar to previous work (Olufsen et al. 2006), i.e., we let $n_i(0) = 0$, $\overline{p}(0) = $ mean (p_i^d $i = 1,\ldots,5$) $dC_i/dt = 0$ which gives that

$$C_{nor}(0) = T_{sym}(0) = \frac{1 - N/M}{1 + \beta N/M} \text{ and } C_{ach}(0) = \frac{N}{M}.$$

13

Finally, the initial value for the heart rate potential $\phi(0) = 0$.

Subject specific parameter values were, as discussed earlier, obtained using Kelley's implementation of the Nelder-Mead method (Kelley 1999). This method is one of many nonlinear optimization methods that can be used to identify model parameters. In part II of this article, we have compared the Nelder-Mead method to implicit filtering and a genetic algorithm.

Sensitivity Analysis

To determine the sensitivity of the states with respect to each of the model parameters we used local sensitivity analysis as described in (Carmichel et al. 1997; Ellwein et al. 2007). Using this analysis we determine how the model states $\overline{x}$ (defined in Eq. 9) change with respect to each of the parameters θ as a function of time, i.e., the goal is to calculate $\partial \overline{x}/\partial \theta_i$. These sensitivities can be found by solving a system of differential equations obtained by implicitly differentiating the state equations in (9) with respect to each of the model parameters in θ, i.e.,

$$\frac{\partial}{\partial \theta_i} \frac{dx}{dt} = \frac{\partial f}{\partial \overline{x}} \frac{\partial \overline{x}}{\partial \theta_i} + \frac{\partial \overline{f}}{\partial \theta_i} \iff \frac{\partial}{\partial t} \frac{dx}{d\theta_i} = \frac{\partial f}{\partial \overline{x}} \frac{\partial \overline{x}}{\partial \theta_i} + \frac{\partial \overline{f}}{\partial \theta_i}.$$

14

The switch in order of differentiation is valid if all concerned derivatives are continuous (Kaplan 1991). Given that $\overline{x} = \{\overline{p}, n_s, n_I, n_L, C_{nor}, C_{ach}, \phi\}$ has seven elements and that θ has 17 elements we get (7×17) differential equations (sensitivity equations), which should be be solved simultaneously with the seven differential equations in (9) that describe the dynamics of the system. Consequently, we need to solve a total of ($7 + 7 \times 17 = 136$) coupled differential equations. When solving these equations, we assume that $\partial \overline{x}/\partial \theta_i(t_0) = 0$, i.e., initially (at time $t = t_0$) we assume that the model does not depend on the parameters. The structure of the sensitivity equations is described in Appendix A.

Data to be analyzed in this study predict heart rate as a function of time, however, we do not have an explicit differential equation predicting heart rate. Heart rate is predicted using an integrate-and-fire model as described above. Furthermore, we do not solve the delay differential equations explicitly, but take advantage of the sequential structure of the model, and first solve for $\{\overline{p}, n_S, n_I, n_L\}$ and then use both $n_i(t)$ and $n_i(t - \tau_d)$ to compute $\{C_{nor}, C_{ach}, \phi\}$. Thus we cannot use the implicit differentiation approach described above to compute the sensitivity to the time-delay τ_d and to the heart rate.

One way to compute sensitivities of all parameters with respect to heart rate and of the delay time with respect to $\{C_{nor}, C_{ach}, \emptyset\}$ is to use finite differences. We do so using a central finite difference scheme in which we calculate

$$\frac{\partial \overline{x}_i}{\partial \theta_j} \approx \frac{\overline{x}_i(\theta_j+h) - \overline{x}_i(\theta_j - h)}{2h},$$

15

which has error $O(h^2)$. This finite difference formula requires two function evaluations or two solves of the state equations: for $\overline{x}_i (\theta - h)$ and for $\overline{x}_i (\theta + h)$. We use this methodology to calculate $\partial HR/\partial \theta_i$, $i = 1,\ldots,17$ and $\partial \overline{x}_i/\partial \tau_d$, $i = C_{nor}, C_{ach}$. The main drawback of this method is the difficulty of analyzing the accuracy of the sensitivity estimates due to the finite-precision arithmetic on a computer. If h is too small in relation to θj we loose most of the significant digits when calculating the difference between two almost equal numbers $\left(\overline{x}_i\left(\theta_j - h\right)\right)$ and $\left(\overline{x}_i\left(\theta_j+h\right)\right)$. On the other hand, if h is so large that $\overline{x}_i\left(\theta_j+h\right) \neq \overline{x}_i\left(\theta_j - h\right)$, the finite difference approximation of the derivative becomes inaccurate. A simple rule (Dennis and Schnable 1983) for the case where $\overline{x}_i$ can be computed accurately to machine precision is to choose $h \approx$ $(macheps)^{1/3}$, *macheps* denotes *machine epsilon*; the smallest positive number ε for, which $1 + \varepsilon > 1$ on the given computer. In our model, $\overline{x}_i$ the solution to the differential equations in (9) is computed using Matlab's differential equations solver *ode15s* with both absolute and relative error tolerances set to 10^{-6}; thus our "*macheps* $= 10^{-6}$". Therefore, in our calculation of the normalized sensitivity functions using central finite difference formula we used $h = 10^{-2}$ to provide a balance between the finiteprecision arithmetic and function evaluation errors.

To rank the sensitivities of the various states and parameters we define a global time-invariant normalized sensitivity using a weighted 2-norm of the form (Sorteleder 1998)

$$z_{ij} = \frac{\theta_j}{\max_{t_0 \leq t \leq t_{end}} |x_i(t,\theta)|} \left(\frac{1}{t_{end}-t_0}\right)$$
$$\times \left\{ \int_{t_0}^{t_{end}} \left|\frac{\partial x_i}{\partial x_j}\right|^2 dt \right\}^{1/2}, \theta_j \neq 0.$$

16

If the matrix $Z = (z_{ij})$ has a row whose elements are all near zero, then the corresponding state variable is not dependent on any of the model parameters. That is, measurements of the corresponding state variable will not contribute to more reliable estimates of the parameters. On the other hand, if the column of the matrix Z is zero, then the corresponding model parameter will have no influence on the model responses and can therefore not be estimated.

It should be noted that the total firing-rate is given by $n = n_S + n_I + n_L + N$; hence, $\partial n/\partial \theta_j = \partial n_S/\partial \theta_j + \partial n_I/\partial \theta_j + \partial n_L/\partial \theta_j$. Therefore, we normalize the sensitivity functions of n with respect to model parameters as $(\theta_j/n - N(\partial n/\partial \theta_j))$. For the other sensitivity variables, we normalize them as described in Eq. 16.

Results

Simulations were carried out for five healthy elderly subjects undergoing two orthostatic stress tests: sit-to-stand and head-up tilt. Demographic and physiologic characteristics are shown in Table 1. Table 2 shows parameter values obtained for each of the five subjects. For each experiment we have included 15–25 s of baseline data followed by either active standing or passive tilt.

We were able to identify model parameters for all subjects and for both tests, but it should be noted that the standard deviation for each of the model parameters is large. Thus making quantitative conclusions based on the small dataset included in this study difficult. For example during sit-to-stand, for subjects II–V we got $k_S = 1.70 \pm 0.27$. However, when including all five subjects we obtained $k_S = 3.50 \pm 4.0$. This result is a consequence of the fact that for subject I $k_S = 10.725$. It may be that subject I is an outlier, it may be that the optimized parameter value represents a local minimum outside the desired parameter range, or it may be that this parameter depend on other model parameters. Two parameters were detected as being significantly different between the two experiments: The parameter η was higher during head-up tilt indicating that the base line firing rate is higher during head-up tilt than during sit-to-stand and the parameter u_0 was lower during head-up tilt indicating that the activation of muscle sympathetic outflow was less pronounced than during sit-to-stand marked with bold in Table 2. In addition, even though parameters varied significantly, the dynamics of the state variables were similar for all five subjects. Figure 4 shows the dynamics for subject I (a healthy female 60 years old) for each of the two experiments, sit-to-stand (left column) and head-up tilt (right column). During sit-to-stand a rapid decline in the blood pressure (a) is accompanied by a decline in the firing-rate (b) and parasympathetic tone (c). In addition it should be noted that sympathetic outflow increase stimulated by vestibular and central command stimulation of muscle sympathetic activity precedes the drop in blood pressure. Consequently, the hysteresis loop (d) shows a fairly rapid decrease followed by a slower recovery. The loop is not closed because blood pressure increases further during standing. Similar to previous work (Olufsen et al. 2006) it should be noted that the hysteresis loop is fairly narrow. Finally, it should be noted that predicted and calculated values of heart rate (e) are closely correlated (the correlation coefficient $R = 0.96$, see Table 2). During head-up tilt (right column) supine blood pressure (a) is lower compared to sitting baseline by 15 mmHg (see Table 1). Line indicates the time when the tilt was completed, but the actual motion of the table begun about 10 s earlier. Blood pressure declines more gradually over approximately 10 s and $\Delta \overline{p}$ is significantly smaller (4.78 versus 19.77 [mmHg]). Consequently, there is a smaller decline in baroreflex firingrate (b). Furthermore, the model shows that parasympathetic outflow declines more gradually or perhaps there is even an initial increase in the response to the increase of sympathetic tone (c). Similar to sit-to-stand, the hysteresis loop (d) is very narrow (and almost linear), but it is shifted toward lower blood pressure values (e). These findings are important because they demonstrate dynamics of the baroreflex activity can be different in response to passive or active postural stimulus. We also show that linear responses is typical for smaller blood pressure change at lower mean values during head-up tilt and an open loop-hysteresis response is more typical for higher blood pressure values and larger involvement of muscle sympathetic activity during active standing. The heart rate response (e) is less pronounced (0.18 versus 0.33 [bps]). Also note the initial drop in heart rate observed at the beginning of the tilt (during the upward motion, marked by an arrow). To our knowledge this last observation has not been well described in previous studies. This effect is not accounted for in our model and thus the correlation between predicted and actual heart rate is less (the correlation coefficient $R = 0.83$ versus $R = 0.94$, see Table 2) during head-up tilt.

Figures 5 and 6 as well as Table 3 show results of our sensitivity analysis, the figures show the normalized sensitivities. Table 3 shows the overall ranking (including all states and all parameters) of sensitivities calculated using Eq. 16. In Fig. 5 we have plotted the ranked sensitivities from the most to the least sensitive. Figure 5a shows the result of the overall ranking while Fig. 5b shows ranking of parameters with respect to heart rate. Notice that this ranking differs from the overall ranking. In this study, we only validate the model against heart rate data, thus the ranking in (b) should be used to guide the parameter estimation process. The most sensitive parameters include $\{\xi_P, \eta, t_{start}, \alpha\}$. Figure 6 shows examples of the time dependent sensitivities for the parameters ranked with respect to heart rate. The figure shows scaled versions of the most (ξ_P), an intermediate (k_S), and the least (τ_I) sensitive parameters.

Panel (a) shows time dependent sensitivities for all three parameters calculated using the optimized parameter values and panels (b–d) show these parameters effect on heart rate. In these panels, the black lines are computed using the optimized parameter values and the grey line represents a 10% increase of the parameter in question. Note that a 10% change in ξ_P gives rise to a significant decrease in HR, while a 10% increase in k_S or in has almost no effect on heart rate.

Discussion

Results show that it is possible to use our previously developed model (Olufsen et al. 2006) to predict heart rate changes during sit-to-stand and head-up tilt. The main contributions from this study were: (i). We were able to predict heart rate for all five subjects and dynamics of the intermediate responses looked similar for all subjects, thus we are able to (at least qualitatively) discuss impact of the model. (ii). We were able to calculate and rank sensitivities. Results of this ranking can be used to estimate how many parameters that can be uniquely identified. (iii). The most important observation is that different dynamics were observed between head-up tilt and sit-to-stand. During sit-to-stand heart rate increased immediately upon preparation to standing, while during head-up tilt heart rate decreased before it started to increase. (iv). This study showed that inclusion of age dependence in initial iterates for parameters used to predict baseline firing-rate and intrinsic heart rate gave rise to better prediction of the overall firing-rate n. Below, we will discuss advantages and limitations for each of these observations.

(*i–ii*): Similar to previous work, we found that our model has potential to be analyzed in more detail, and results from this study have enabled us to identify several important features. First, we noticed that parameters varied significantly between subjects while the dynamics (illustrated in Fig. 4) follow similar trends. There are several reasons for the discrepancies observed in the parameter values. The parameter estimation methods are local, thus, there is no guarantee that the parameters identified represent the absolute minimal cost, and even if a minimal cost has been obtained the optimization may have identified a parameter outside the physiological range. Second, we used the Nelder–Mead optimization method (a simplex method), which do not allow us to constrain parameters. Furthermore, we try to identify a large number (17) of parameters, which may not all be identifiable. In fact, results of our sensitivity analysis showed that at least three parameters are unidentifiable. Finally, model parameters may depend on each other. To understand our results better, we have analyzed several optimization methods. Results of this study are discussed in part II of this manuscript.

(*iii*): Probably the most important observation gained from this study is that while the model displays excellent fits to the sit-to-stand data, four out of five subjects showed a decrease in heart rate during head-up tilt. These changes most likely reflect reductions of intracranial pressure and increases in central venous pressure in the right atrium, which, in turn, lead to increases in cardiac output and the observed decrease in heart rate. These results may stem from the hydrostatic pressure changes opposed during headup tilt, which are different than the ones observed during sit-to-stand. During head-up tilt, the head is slowly moved to a location above the heart, while during sit-to-stand no hydrostatic pressure changes are enforced between the head and the heart. Notice that during standing (or during sitting) the hydrostatic pressure in the head is approximately 10 mmHg less than in the heart (Guyton and Hall 1996).

(*iv*): Another difference between our previous study and this study is that we adjusted intrinsic and maximum heart rates to age. These adjustments are physiological, it is well known that adaptation to orthostatic stress, mainly parasympathetic withdrawal, declines with age. This relative minor change had a fairly significant effect on the dynamics, in particular, for the dynamics of the overall firing-rate n, as well as on parasympathetic and sympathetic outflows, which are proportionally and inverse proportionally related to the firing-rate. This is a

significant improvement over our previous study (Olufsen et al. 2006), where for most subjects, the steady-state baroreflex firing-rate was close to the maximal firing-rate.

A limitation of this study is that our model only included an empirical description of the combined effect of vestibular and central command stimulation of muscle sympathetic nerve activity, which may likely be activated differently during tilt than during sit-to-stand. It is interesting though, that sympathetic activation occurs approximately at the same time in both conditions and with a similar amplitude. One way to address this further would be to develop a biophysical model for this response. Also, it should be noted that the tilt study was done on an automatic tilt-table, which uses an electrical engine to tilt the table to 70°. While this automated tilt-table allows for a more accurate tilt angle, it has the disadvantage that the tilting process is fairly slow, it takes about 5 s to tilt the subject to upright position. This relatively slow tilt time has an effect on the immediate drop in blood pressure, since, in particular, parasmpathetic response acts within this time-frame and thus already is activated before the subject is fully tilted, thus preventing a more drastic blood pressure drop.

Acknowledgments

Appendix A

Sensitivity Equations

The model presented in (1–8) includes five state equations with a total of 17 model parameters. To derive sensitivity equations we differentiate each of the states with respect to each of the parameters, except for the delay parameter τd for which sensitivities will be computed using central finite differences as described in (15). Because the system is coupled in the forward direction, parameter dependence carries through the model. The five state equations depend on the 17 parameters as follows:

$$
\begin{aligned}
&\overline{p}(\alpha) \\
&n(\alpha, k_i, \tau_i, \eta), \ i{=}S, I, L \\
&C_{ach}(\alpha, k_i, \tau_i, \eta, \tau_{ach}), \ i{=}S, I, L \\
&C_{nor}(\alpha, k_i, \tau_i, \eta, \tau_{nor}, \tau_d, u_0, t_{start}, t_{per}, \beta), \ i{=}S, I, L \\
&\phi(\alpha, k_i, \tau_i, \eta, \tau_{ach}, \tau_{nor}, \tau_d, u_0, t_{start}, t_{per}, \beta, \xi_s, \xi_p), \\
&i{=}S, I, L.
\end{aligned}
\tag{A1}
$$

Mean Pressure

The mean pressure was modeled using the differential equation in (1), which depends on one parameter α.

$$\frac{\mathrm{d}p}{\mathrm{d}t}=\alpha(p-\overline{p}).$$

<div align="right">A2</div>

Thus, only one sensitivity equation can be formed, namely

$$\frac{\mathrm{d}}{\mathrm{d}t}\left(\frac{\partial\overline{p}}{\partial\alpha}\right)=\frac{\partial}{\partial\alpha}\left(\frac{\mathrm{d}p}{\mathrm{d}t}\right)=p-\overline{p}-\alpha\frac{\partial\overline{p}}{\partial\alpha}.$$

<div align="right">A3</div>

Baroreflex Firing Rate

The baroreflex firing rate is combined of three firing rates ni as described in Eqs. 2-3. These equations were given by

$$\frac{\mathrm{d}n_i}{\mathrm{d}t}=k_i\frac{\mathrm{d}p}{\mathrm{d}t}\frac{n(M-n)}{(M/2)^2}-\frac{n_i}{\tau_i},\ \ i=S,I,L$$
$$n=n_s+n_I+n_L+N,\ \ N=\frac{M}{2}\left(1+\frac{\eta^2}{1+\eta^2}\right).$$

<div align="right">A4</div>

These three differential equations depend on eight parameters α, k_i, τ_i, η, for $i = S, I, L$. Thus we get $3 \times 8 = 24$ sensitivity equations.

1. For the parameter α:

$$\frac{\mathrm{d}}{\mathrm{d}t}\left(\frac{dn_i}{\partial\alpha}\right)=\frac{\partial}{\partial\alpha}\left(\frac{\partial n_i}{\mathrm{d}t}\right)$$
$$=k_i\left[\frac{\mathrm{d}p}{\mathrm{d}t}\frac{\partial n}{\partial\alpha}\frac{M-2n}{(M/2)^2}+\frac{\partial}{\partial\alpha}\frac{\mathrm{d}p}{\mathrm{d}t}\frac{n(M-n)}{(M/2)^2}\right]-\frac{1}{\tau_i}\frac{\partial n_i}{\partial\alpha}$$
$$\frac{\mathrm{d}}{\mathrm{d}t}\left(\frac{\partial n_i}{\partial\eta}\right)=\frac{\partial}{\partial\eta}\left(\frac{\mathrm{d}n_i}{\mathrm{d}t}\right)=k_i\frac{\mathrm{d}p}{\mathrm{d}t}\frac{\partial n}{\partial\eta}\frac{M-2n}{(M/2)^2}-\frac{1}{\tau_i}\frac{\partial n_i}{\partial\eta}.$$

<div align="right">A5</div>

2. For $i = j$, $i \in \{S, I, L\}$:

$$\frac{\mathrm{d}}{\mathrm{d}t}\left(\frac{\partial n_i}{\partial k_j}\right)=\frac{\mathrm{d}}{\mathrm{d}t}\left(\frac{\partial n_i}{\partial k_i}\right)=\frac{\partial}{\partial k_i}\left(\frac{\partial n_i}{\mathrm{d}t}\right)=\frac{\mathrm{d}p}{\mathrm{d}t}\left(\frac{n(M-n)}{(M/2)^2}+k_i\frac{\partial n}{\partial k_i}\frac{M-2n}{(M/2)^2}\right)-\frac{1}{\tau_i}\frac{\partial n_i}{\partial k_i}$$
$$\frac{\mathrm{d}}{\mathrm{d}t}\left(\frac{\partial n_i}{\partial\tau_j}\right)=\frac{\mathrm{d}}{\mathrm{d}t}\left(\frac{\partial n_i}{\partial\tau_i}\right)=\frac{\partial}{\partial\tau_i}\left(\frac{\partial n_i}{\mathrm{d}t}\right)=k_i\frac{\mathrm{d}p}{\mathrm{d}t}\frac{\partial n}{\partial\tau_i}\frac{M-2n}{(M/2)^2}+\frac{n_i}{\tau_i^2}-\frac{1}{\tau_i}\frac{\partial n_i}{\partial\tau_i}.$$

<div align="right">A6</div>

3. For $i \neq j$, $j \in \{S, I, L\}$, $y = \{k_j, s_j\}$:

$$\frac{\mathrm{d}}{\mathrm{d}t}\left(\frac{\partial n_i}{\partial\gamma_j}\right)=\frac{\partial}{\partial\gamma_j}\left(\frac{\mathrm{d}n_i}{\mathrm{d}t}\right)=k_i\frac{\mathrm{d}p}{\mathrm{d}t}\frac{\partial n}{\partial\gamma_j}\frac{M-2n}{(M/2)^2}-\frac{1}{\tau_i}\frac{\partial n_i}{\partial\gamma_j}.$$

<div align="right">A7</div>

Acetylcholine Concentration

The concentration of acetylcholine was modeled using a first order set-point equation as described in (6).

$$\frac{dC_{ach}}{dt} = \frac{-C_{ach} + T_{par}}{\tau_{ach}}, \quad T_{par} = \frac{n}{M},$$
$$n = n_S + n_I + n_L + N, \quad N = \frac{M}{2}\left(1 + \frac{\eta^2}{1+\eta^2}\right).$$

A8

This equation depends on nine parameters α, k_i, τ_i, η, η_{ach}, for $i = S, I, L$. Thus we formulate $1 \times 9 = 9$ sensitivity equations. For $\gamma = \{\alpha, k_i, \tau_i, \eta\}$, $i = S, I, L$ the sensitivity equations have the form:

$$\frac{d}{dt}\left(\frac{\partial C_{ach}}{\partial \gamma_i}\right) = \frac{\partial}{\partial \gamma_i}\left(\frac{dC_{ach}}{dt}\right) = \frac{1}{\tau_{ach}}\left(-\frac{\partial C_{ach}}{\partial \gamma_i} + \frac{1}{M}\frac{\partial n}{\partial \gamma_i}\right).$$

A9

The sensitivity equation for τ_{ach} is given by

$$\frac{d}{dt}\left(\frac{\partial C_{ach}}{\partial \tau_{ach}}\right) = \frac{\partial}{\partial \tau_{ach}}\left(\frac{dC_{ach}}{dt}\right) = -\frac{1}{\tau_{ach}}\frac{\partial C_{ach}}{\partial \tau_{ach}} + \frac{C_{ach} - T_{par}}{\tau_{ach}^2}.$$

A10

Noradrenaline Concentration

The noradrenaline concentration was also modeled using the first-order set-point equation described in (6). Accounting for vestibular stimulation of muscle sympathetic activation and central command this equation was given by

$$\frac{dC_{nor}}{dt} = \frac{-C_{nor} + T_{sym}}{\tau_{nor}}, \quad T_{sym}\frac{T_s}{1+\beta T_{par}}, \quad T_s = 1 - \frac{n(t - \tau_d)}{M} + u, \quad T_{par} = \frac{n(t)}{M}.$$

A11

In the above equation u denote an impulse function accounting for vestibular feedback. This function was given by

$$u = -[b(t - t_m)]^2 + u_0, \quad b = \sqrt{\frac{4u_0}{t_{per}^2}}, \quad t_m = t_{start} + \frac{t_{per}}{2} \iff$$
$$u = u_0 - \frac{4u_0(t - t_{start} - 0.5t_{per})2}{t_{per}^2}.$$

A12

This one differential equation has 14 parameters. Thus we get additional 14 sensitivity equations. For $\gamma = \{\alpha, k_i, \tau_i, \eta\}$, $i = S, I, L$ we get sensitivity equations of the form:

$$\frac{d}{dt}\left(\frac{\partial C_{nor}}{\partial \gamma_i}\right) = \frac{\partial}{\partial \gamma_i}\left(\frac{dC_{nor}}{dt}\right) = \frac{1}{\tau_{nor}}$$
$$\left[-\frac{\partial C_{nor}}{\partial \gamma_i} - \frac{1}{(1+\beta T_{par})^2}\left(\frac{1+\beta T_{par}}{M}\frac{\partial n(t-\tau_d)}{\partial \gamma_i} + \frac{T_s\beta}{M}\frac{\partial n}{\partial \gamma_i}\right)\right].$$

A13

The remaining six sensitivity equations are given by

Heart Rate Potential

The heart rate potential ø in (7) was modeled using the differential equation

$$\frac{d}{dt}\left(\frac{\partial C_{nor}}{\partial \tau_{nor}}\right) = \frac{\partial}{\partial \tau_{nor}}\left(\frac{dC_{nor}}{dt}\right) = -\frac{1}{\tau_{nor}}\frac{\partial C_{nor}}{\partial \tau_{nor}} + \frac{C_{nor} - T_{sym}}{\tau_{nor}^2}$$

$$\frac{d}{dt}\left(\frac{\partial C_{nor}}{\partial \tau_d}\right) = \frac{\partial}{\partial \tau_d}\left(\frac{dC_{nor}}{dt}\right) = \frac{1}{\tau_{nor}}\left[-\frac{\partial C_{nor}}{\partial \tau_d} - \frac{1}{M(1+\beta T_{par})}\frac{\partial n(t-\tau_d)}{\partial \tau_d}\right]$$

$$\frac{d}{dt}\left(\frac{\partial C_{nor}}{\partial u_0}\right) = \frac{\partial}{\partial u_0}\left(\frac{dC_{nor}}{dt}\right) = \frac{1}{\tau_{nor}}\left[-\frac{\partial C_{nor}}{\partial u_0} + \frac{1}{1+\beta T_{par}}\left(1 - \frac{4(t-t_{start}-0.5t_{per})^2}{t_{per}^2}\right)\right]$$

$$\frac{d}{dt}\left(\frac{\partial C_{nor}}{\partial t_{start}}\right) = \frac{\partial}{\partial t_{start}}\left(\frac{dC_{nor}}{dt}\right) = \frac{1}{\tau_{nor}}\left[-\frac{\partial C_{nor}}{\partial t_{start}} + \frac{8u_0(t-t_{start}-0.5t_{per})^2}{(1+\beta T_{par})t_{per}^2}\right]$$

$$\frac{d}{dt}\left(\frac{\partial C_{nor}}{\partial t_{per}}\right) = \frac{\partial}{\partial t_{per}}\left(\frac{dC_{nor}}{dt}\right) = \frac{1}{\tau_{nor}}\left[-\frac{\partial C_{nor}}{\partial t_{pd}} + \frac{4u_0}{1+\beta T_{par}}\left(\frac{2(t-t_{start}-0.5t_{per})^2}{t_{per}^3} + \frac{t-t_{start}-0.5t_{per}}{t_{per}^2}\right)\right]$$

$$\frac{d}{dt}\left(\frac{\partial C_{nor}}{\partial \beta}\right) = \frac{\partial}{\partial \beta}\left(\frac{dC_{nor}}{dt}\right) = \frac{1}{\tau_{nor}}\left(-\frac{\partial C_{nor}}{\partial \beta} - \frac{T_s T_{par}}{(1+\beta T_{par})^2}\right).$$

A14

$$\frac{d\phi}{dt} = H_0(1 + M_s C_{nor} - M_p C_{ach}),$$
$$M_s = \frac{\xi_s^2}{1+\xi_s^2}, \quad M_p = \frac{\xi_s^2}{1+\xi_s^2}.$$

A15

This equation depends on all 17 model parameters. It should be noted that H_0 is not a parameter but is determined directly as a function of age as described above. Thus, this differential equation gives rise to the following 17 sensitivity equations. Only the parameters ξ_s and ξ_p appear directly in the equation. Parameters $\gamma = \{\alpha, k_i, \tau_i, \eta\}$, $i \in \{S, I, L\}$ appear in both C_{nor} and C_{ach} thus sensitivities with respect to these parameter have the form

$$\frac{d}{dt}\left(\frac{\partial \phi}{\partial \gamma_j}\right) = \frac{\partial}{\partial \gamma_j}\left(\frac{\partial \phi}{\partial t}\right) = H_0\left(M_s \frac{\partial C_{nor}}{\partial \gamma_j} - M_p \frac{\partial C_{ach}}{\partial \gamma_j}\right).$$

A16

C_{ach} also depend on τ_{ach}, which gives rise to the sensitivity equation

$$\frac{d}{dt}\left(\frac{\partial \phi}{\partial \tau_{ach}}\right) = \frac{\partial}{\partial \tau_{ach}}\left(\frac{d\phi}{dt}\right) = -H_0 M_p \frac{\partial C_{ach}}{\partial \tau_{ach}}.$$

A17

Furthermore, C_{nor} depends on parameters $\lambda = \{\tau_{nor}, \tau_d, u_0, t_{start}, t_{per}, \beta\}$, which gives sensitivity equations on the form

$$\frac{d}{dt}\left(\frac{\partial \phi}{\partial \lambda_i}\right) = \frac{\partial}{\partial \lambda_i}\left(\frac{\partial \phi}{\partial t}\right) = H_0 M_s \frac{\partial C_{nor}}{\partial \lambda_i}.$$

A18

Only two additional sensitivity equations needs to be derived, namely for ξ_s and ξ_p. These are given by

$$\frac{\mathrm{d}}{\mathrm{d}t}\left(\frac{\partial\phi}{\partial\xi_i}\right)=\frac{\partial}{\partial\xi_i}\left(\frac{\partial\phi}{\partial t}\right)=H_0 C_{nor}\frac{2\xi_i}{(1+\xi_i^2)^2}, i=s,p.$$

A19

Again, it should be noted that the final sensitivities with respect to heart rate and to the delay parameter τd are computed using finite differences as described in (15).

References

Carmichel G, Sandu A, et al. Sensitivity analysis for atmospheric chemistry models via automatic differentiation. Atmos Environ 1997;31:475–89.

Cecchini A, Tiplitz K, et al. Baroreceptor activity related to cell properties. Proc 35th Ann Conf Med Biol 1982;24

Danielsen M, Ottensen J. A dynamical approach to the baroreceptor regulation of the cardiovascular system. Proc 5th Int Symp, Symbiosis 1997:25–29.

Dennis, J.; Schnable, R. Numerical methods for unconstrained optimization and nonlinear equations. Englewood Cliffs: Prentice Hall Inc; 1983.

Ellwein L, Tran H, et al. Sensitivity analysis and model assessment: mathematical models for arterial blood flow and blood pressure. J Cardiovasc Eng. (this issue). doi: 10.1007/s10558-007-9047-3

Franz G. Nonlinear rate sensitivity of carotid sinus reflex as a consequence of static and dynamic nonlinearities in baroreceptor behavior. Ann NY Acad Sci 1969;156:811–24. [PubMed: 5258020]

Guyton, A.; Hall, J. Textbook of medical physiology. Philadelphia: WB Saunders; 1996.

Johnson P, Shore A, et al. Baroreflex sensitivity measured by spectral and sequence analysis in cerebrovascular disease: methodological considerations. Clin Auton Res 2006;16:270–5. [PubMed: 16770526]

Jose A, Collison D. The normal range and determinants of the intrinsic heart rate in man. Cardiovasc Res 1970;4:160–7. [PubMed: 4192616]

Kaplan, W. Advanced calculus. Rdwood City CA: Addison Wesley Publishing Company; 1991.

Kaufmann H, Biaggioni I, et al. Vestibular control of sympathetic activity: an otolith-sympathetic reflex in humans. Exp Brain Res 2002;143:463–9. [PubMed: 11914792]

Kelley, C. Iterative methods for optimization. Philadelphia: SIAM; 1999.

Levy M, Zieske H. Autonomic control of cardiac pacemaker. J Appl Physiol 1969;27:465–70. [PubMed: 5822553]

Low, P. Clinical autonomic disorders: evaluation and management. Philadelphia: Lippincott Williams & Wilkins; 1997.

Olufsen M, Tran H, et al. Modeling baroreflex regulation of heart rate during orthostatic stress. Am J Physiol 2006;291:R1355–68.

Opthof T. The normal range and determinants of the intrinsic heart rate in man. Cardiovasc Res 2000;45:173–6. [PubMed: 10728332]

Ottesen J. Nonlinearity of baroreceptor nerves. Surv Math Ind 1997;7:187–201.

Poitras J, Pantelakis N, et al. Analysis of the blood pressure – baroreceptor nerve firing relationship. Proc 19th Ann Conf Eng Med Biol 1966:8–105.

Ray C. Interaction of the vestibular system and baroreflexes on sympathetic nerve activity in humans. Am J Physiol 2000;279:H2399–404.

Ray C, Carter J. Vestibular activation of sympathetic nerve activity. Acta Physiol Scand 2003;177:313–9. [PubMed: 12609001]

Ray C, Monahan K. The vestibulosympathetic reflex in humans: neural interactions between cardiovascular reflexes. Clin Exp Pharmacol Physiol 2002;29:98–102. [PubMed: 11906466]

Robbe H, Mulder L, et al. Assessment of baroreceptor reflex sensitivity by means of spectral analysis. Hypertension 1987;10:538–43. [PubMed: 3666866]

Robertson, D.; Biaggioni, I., et al. Primer on the autonomic nervous system. Boston: Academic Press; 2005.

Shampine L, Reichelt M. The MATLAB ODE suite. SIAM J Sci Comput 1997;18:1–22.

Shampine L, Reichelt M, et al. Solving index-1 DAEs in MATLAB and Simulink. SIAM Rev 1999;41:538–52.

Smith, J.; Kampine, J. Circulatory physiology, the essentials. Baltimore: Williams and Wilkins; 1990.

Sorteleder, W. Parameter estimation in nonlinear dynamical systems Amsterdam. Netherlands: Stichting Mathematisch Centrum; 1998.

Spickler J, Kedzi P. Dynamic response characteristics of carotid sinus baroreceptors. Am J Physiol 1967;212(2):472–6. [PubMed: 6018034]

Srinivasen R, Nudelman H. Modeling the carotid sinus baroreceptor. Biophys J 1972;12:1171–82. [PubMed: 5056961]

Strobel J, Epstein A, et al. Nonpharmacologic validation of the intrinsic heart rate in cardiac transplant recipients. J Interv Card Electrophysiol 1999;3:15–8. [PubMed: 10354971]

Taher M, Cecchini A, et al. Baroreceptors responses derived from a fundamental concept. Ann Biomed Eng 1988;16:429–43. [PubMed: 3189973]

Wilson T, Cotter L, et al. Vestibular inputs elicit patterned changes in limb blood flow in conscious cats. J Physiol 2006;575:671–84. [PubMed: 16809368]
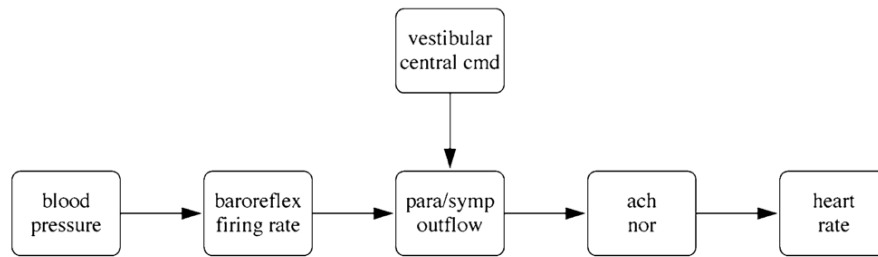
Fig. 1.
Model diagram. The model uses blood pressure as an input to predict baroreflex firing rate. From this we predict sympathetic and parasympathetic outflows, accounting for vestibular stimulation of muscle sympathetic and central command systems. These outflows give rise to changes in concentrations of noradrenaline (nor) and acetylcholine (ach), which in turn gives rise to heart rate changes
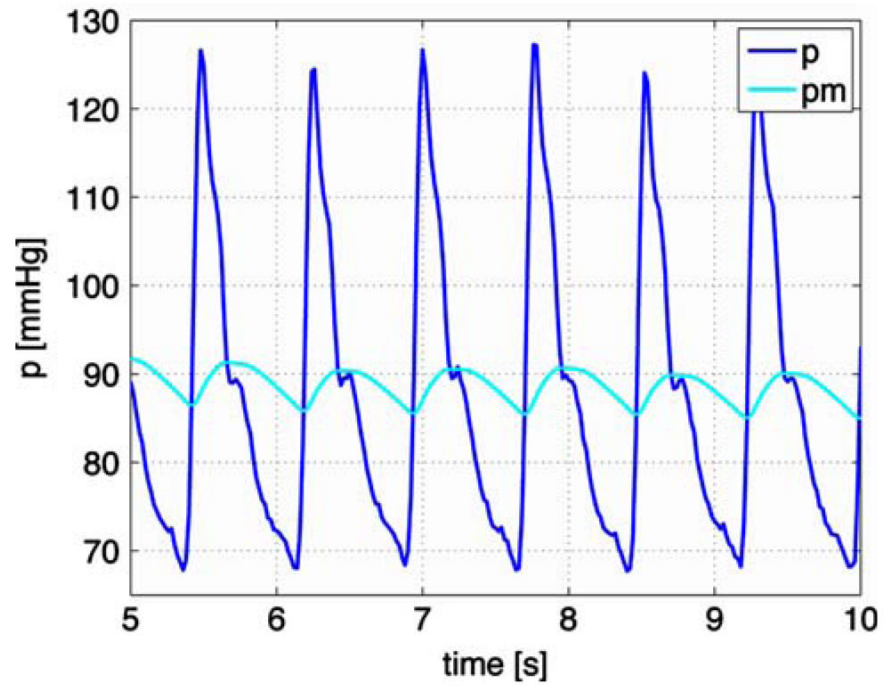
Fig. 2.
Actual (black line) and mean (grey line) blood pressure [mmHg]. The actual blood pressure is obtained directly from data (down-sampled to 50 Hz). The mean blood pressure is calculated using (1) as an average running mean that is continuous in time
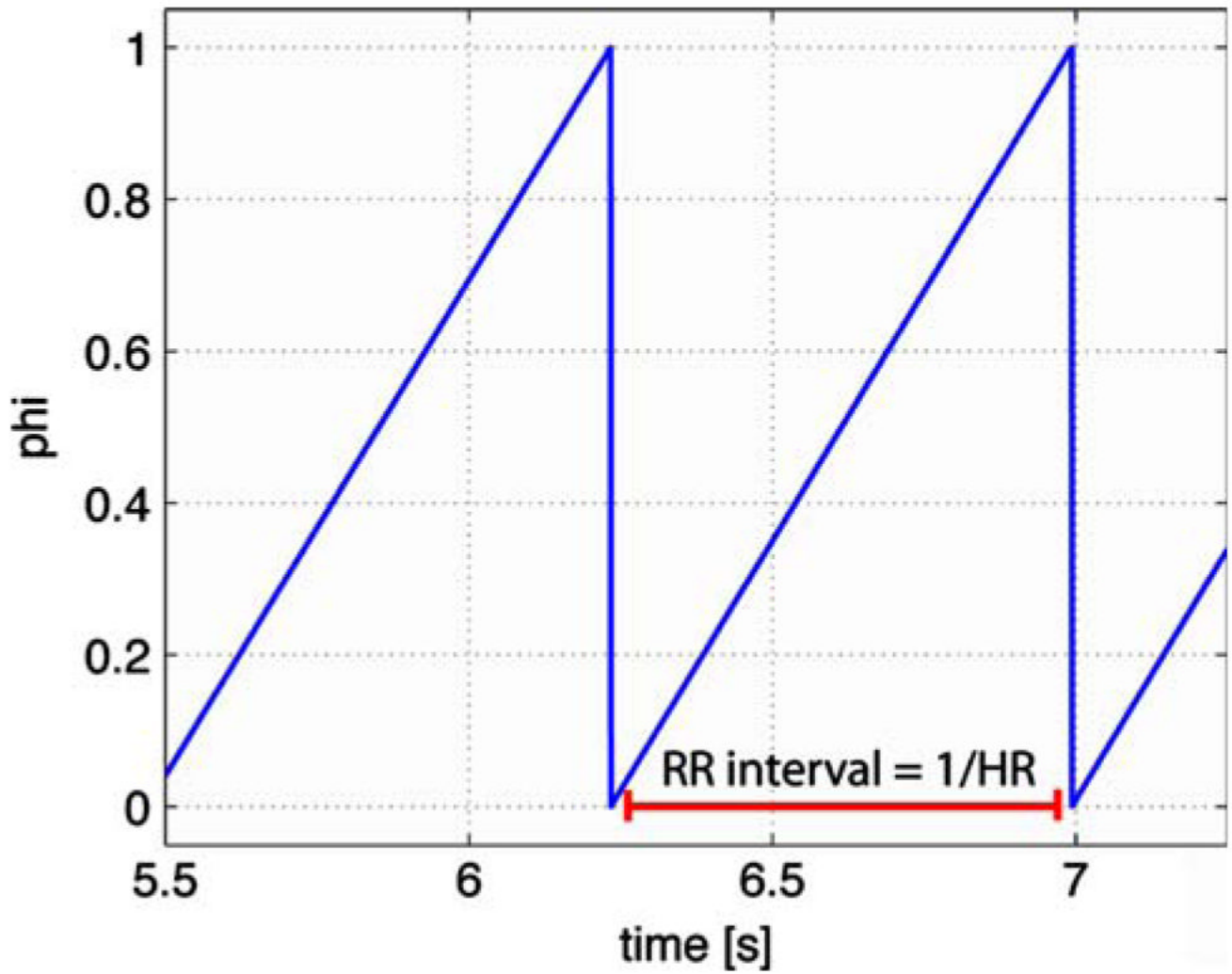
Fig. 3.
The heart rate potential ø. We use an "integrate and fire" model to predict the heart rate potential ø, when the potential reaches one it is reset to 0 and the heart rate (1/RR interval) is computed as the time elapsed since the potential was last reset to 0
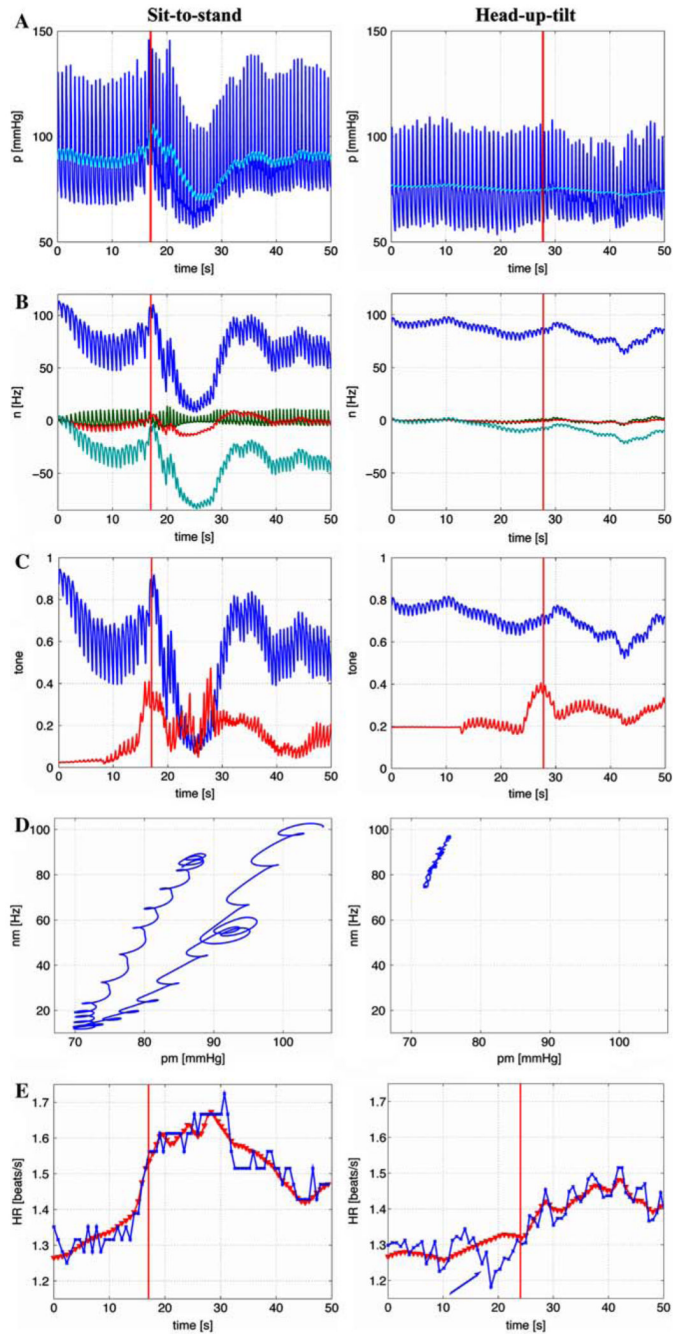
Fig. 4.
Model results for a typical subject, the left column shows response to sit-to-stand while the right column shows the response to head-up tilt. The first row shows the input blood pressure (black line) and the computed average mean blood pressure (grey line). The second row shows the baroreflex firing rate. The bottom three lines shows each of the three components (n_S, n_I, n_L) and the top line shows the combined response $n = n_S + n_I + n_L + N$ including the baseline response N. The third row shows the parasympathetic (top line) and sympathetic (bottom line) response. The fourth row shows the mean firing rate as a function of mean blood pressure. Finally, the last row shows computed (line with triangles) and measured (black line with stars) values of heart rate as a function of time
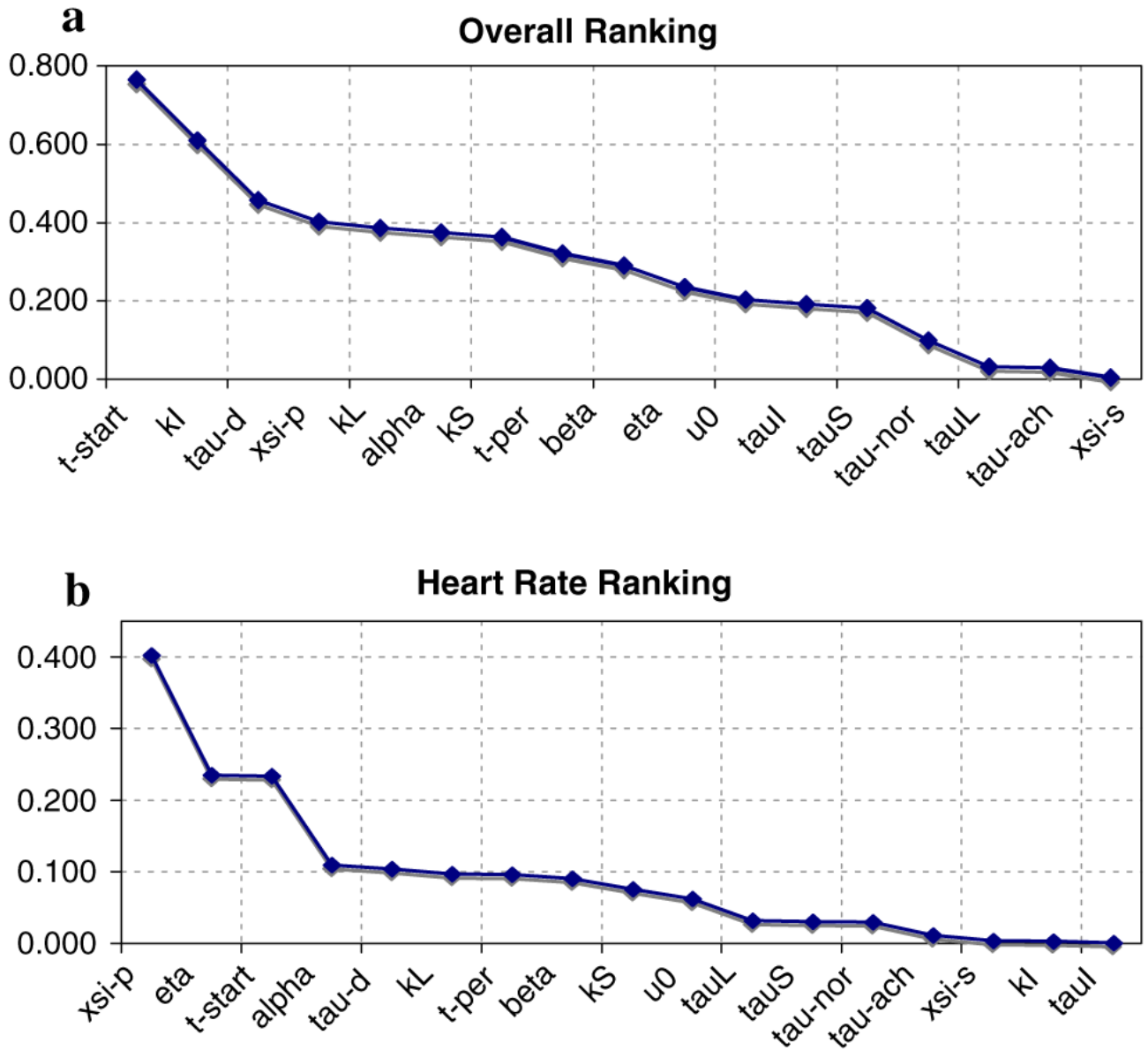
Fig. 5.
This figure shows relative sensitivities for the parameters $\theta_i = \xi_P, k_S, \tau_I$, where ξ_P is the most sensitive parameter, k_S is an intermediate sensitivity parameter, and τ_I is the least sensitive parameter (see Fig. 6)

Fig. 6.
Panel (**a**) shows ranked sensitivities with respect to heart rate for parameters ξ_P, k_S, τ_P. Panels (**b–d**) show heart rate dynamics computed with optimized parameters (dark lines) and with a 10% increase (grey lines) for each of the three parameters

Table 1

Physiological characteristics for the five subjects

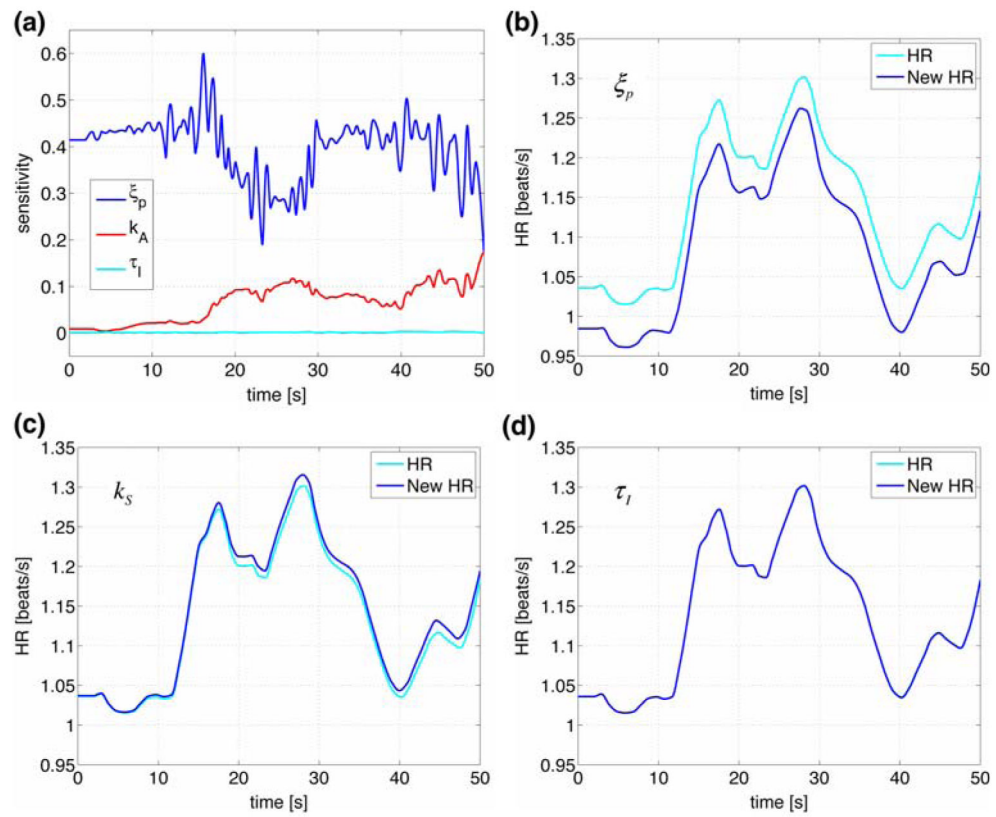|	I	II	III	IV	V	Mean
HR sitting	1.31 ± 0.03	0.94 ± 0.04	1.28 ± 0.03	1.03 ± 0.06	1.06 ± 0.03	1.14 ± 0.16
HR supine	1.30 ± 0.05	0.94 ± 0.03	1.25 ± 0.08	1.00 ± 0.05	1.00 ± 0.03	1.12 ± 0.16
HR standing	1.55 ± 0.09	1.07 ± 0.04	1.49 ± 0.11	1.17 ± 0.08	1.25 ± 0.09	1.31 ± 0.22
HR tilt	1.44 ± 0.04	0.96 ± 0.03	1.46 ± 0.06	1.07 ± 0.05	1.16 ± 0.06	1.26 ± 0.20
ΔHR sit-to-stand	0.33	0.16	0.37	0.59	0.29	0.35 ± 0.16
ΔHR supine-to-tilt	0.18	0.04	0.28	0.46	0.24	0.24 ± 0.15
BP sitting	89.90 ± 17.85	98.30 ± 21.84	105.99 ± 20.09	72.27 ± 19.40	91.17 ± 11.73	92.24 ± 22.98
BP supine	75.29 ± 14.97	78.05 ± 21.81	76.56 ± 19.41	79.23 ± 21.61	79.94 ± 14.38	77.53 ± 18.98
BP standing	87.23 ± 18.40	97.21 ± 26.88	99.65 ± 25.02	74.65 ± 22.41	90.88 ± 15.92	89.92 ± 23.83
BP tilt	74.00 ± 12.20	80.08 ± 19.86	78.33 ± 17.19	81.45 ± 18.27	71.36 ± 13.87	77.53 ± 18.98
ΔBP sit-to-stand	19.77	33.76	43.01	20.31	25.41	28.45 ± 9.89
ΔBP supine-to-tilt	4.78	28.20	28.00	5.71	18.92	17.12 ± 11.48

The first four rows give mean values for heart rate data [beats/s] during sitting, supine, standing, and tilt positions. The next two rows gives the maximum change observed between baseline (sitting or supine) and standing or tilt, respectively. The last six rows provide the same measures for the mean blood pressure data

Table 2

Optimized model parameters for all five subjects with means and standard deviations

Param	Init val	Sit-to-stand I	II	III	IV	V	Mean	Head-up-tilt I	II	III	IV	V	Mean	P value
k_S	2.0	10.725	1.410	1.923	1.519	1.930	3.50 ± 4.0	4.251	1.296	5.785	2.209	1.728	3.05 ± 1.9	0.82
k_I	1.5	1.315	0.473	0.567	0.080	1.205	0.73 ± 0.5	1.594	0.067	1.582	0.003	0.344	0.72 ± 0.8	0.98
k_L	2.0	3.767	0.255	0.515	1.446	1.063	1.41 ± 1.4	5.351	0.146	1.835	3.741	0.778	2.37 ± 2.2	0.43
τ_S	1.0	0.033	0.699	1.414	0.851	1.110	0.82 ± 0.5	1.983	2.852	0.008	1.722	0.273	1.37 ± 1.2	0.38
τ_I	5.0	7.344	5.915	2.841	4.406	7.414	5.58 ± 2.0	9.808	4.702	4.903	6.608	5.468	6.30 ± 2.1	0.59
τ_L	250.0	286.420	262.190	266.414	248.767	246.352	262.03 ± 16	217.65	252.53	255.65	261.45	243.76	246.2 ± 17	0.17
τ_{nor}	1.0	3.406	1.612	1.548	1.762	3.741	2.41 ± 1.1	5.060	0.989	24.919	2.559	2.523	7.21 ± 10	0.32
τ_{ach}	1.0	1.317	3.169	0.795	0.911	3.952	2.03 ± 1.4	0.059	1.642	3.369	2.274	5.032	2.48 ± 1.9	0.68
α	1.0	0.932	2.396	3.068	1.260	4.046	2.34 ± 1.3	0.143	1.925	2.055	0.857	2.592	1.59 ± 1.0	0.29
η	–	1.827	0.970	1.158	1.249	1.196	**1.28 ± 0.3**	1.106	2.885	2.193	1.396	3.668	**2.25 ± 1.1**	**0.08**
ξ_s	–	8.273	5.777	9.084	9.024	6.095	7.65 ± 1.6	8.002	6.909	4.065	4.924	7.866	6.35 ± 1.8	0.26
ξ_p	–	0.389	1.081	0.470	0.927	0.810	0.78 ± 0.3	0.763	0.701	0.447	0.881	0.710	0.70 ± 0.2	0.57
u_0	1.0	1.015	0.387	0.698	0.596	3.435	**1.14 ± 1.3**	0.170	0.033	0.498	0.242	0.160	**0.22 ± 0.2**	**0.16**
t_{start}	15.0	14.412	12.020	14.383	11.025	12.565	–	14.089	19.135	16.175	14.699	15.562	–	–
t_{per}	5.0	5.210	4.702	6.839	7.141	4.312	5.64 ± 1.3	6.102	9.655	3.035	6.637	10.722	7.23 ± 3.1	0.31
τ_d	7.0	8.136	9.661	5.859	6.766	6.869	7.46 ± 1.5	12.559	6.331	1.658	6.163	12.095	7.77 ± 4.6	0.99
β	1.0	4.180	1.401	0.839	1.754	5.960	2.83 ± 2.2	0.192	0.223	2.201	2.294	2.023	1.39 ± 1.1	0.22
Iterations		1587	1463	979	1412	1215	1331 ± 238	1286	822	1175	904	1204	1078 ± 203	–
J		1.30E-3	6.87E-4	1.70E-3	1.80E-3	6.7E-4	1.2E-3 ± 5.4E-4	1.40E-3	5.50E-4	5.80E-4	8.93E-4	3.41E-4	1.8E-3 ± 2.3E-3	–
R		0.96	0.92	0.95	0.90	0.97	0.94 ± 0.03	0.90	0.58	0.79	0.89	0.98	0.83 ± 0.15	0.13

The last three rows show the number of iterations needed for the Nelder–Mead method to converge, the least squares cost J at time of convergence, and the correlation coefficient between computed and measured values of heart rate

Numbers in bold indicate paramets that are significantly different between the two tasks

Table 3

Maximum sensitivities for each state with respect to each parameter
Bold entries indicate the most sensitive state for that given parameter

	P	n_S	n_I	n_L	n	C_{ach}	C_{nor}	ø	HR	Max
t_{start}							**0.766**	0.016	0.234	0.766
k_I		0.002	**0.610**	0.004	0.018	0.007	0.011	0.002	0.003	0.610
τ_d							**0.457**	0.014	0.105	0.457
ξ_p							0.266		**0.403**	0.403
k_L		0.037	0.042	**0.386**	0.312	0.128	0.187	0.043	0.098	0.386
α	0.039	0.322	0.215	**0.374**	0.353	0.130	0.182	0.053	0.110	0.374
k_S		**0.363**	0.068	0.234	0.236	0.092	0.127	0.036	0.077	0.363
t_{per}							**0.321**	0.024	0.097	0.321
β							**0.290**	0.054	0.091	0.290
η		0.158	0.141	0.179	0.169	0.064	0.086	0.015	**0.235**	0.235
u_0							**0.203**	0.023	0.063	0.203
τ_I		0.002	**0.192**	0.001	0.005	0.002	0.003	0.000	0.001	0.192
τ_S		**0.182**	0.009	0.006	0.052	0.021	0.025	0.001	0.031	0.182
τ_{nor}							**0.099**	0.003	0.030	0.099
τ_L		0.022	0.011	0.018	0.008	0.003	0.005	0.001	**0.032**	0.032
τ_{ach}						**0.028**		0.001	0.012	0.028
ξ_s								0.002	**0.004**	0.004

Table 4

A list and explanation of all state variables and model parameters

States	Description	Parameters	Description
p	Weighted mean pressure	α	Weight parameter (for mean pressure)
n_S	Short term baroreceptor firing rate	k_S	Gain constant for short term firing rate
n_I	Intermediate baroreceptor firing rate	k_I	Gain constant for intermediate firing rate
n_L	Long term baroreceptor firing rate	k_L	Gain constant for long term firing rate
C_{ach}	Acetylcholine concentration	τ_S	Time constant for short term firing rate
C_{nor}	Noradrenaline concentration	τ_I	Time constant for intermediate firing rate
$\varnothing$	Heart rate potential	τ_L	Time constant for long term firing rate
		η	Scaling factor for baseline firing rate
		β	Parasympathetic dampening factor
		u_0	Amplitude of impulse function
		t_{start}	Start time of impulse function
		t_{per}	Duration of impulse function
		τ_d	Time delay constant for sympathetic tone
		τ_{nor}	Noradrenaline time scale
		τ_{ach}	Acetylcholine time scale
		ξ_s	Scaling factor for sympathetic response
		ξ_p	Scaling factor for parasympathetic response